Novel Electronic and Magnetic Properties of Two-Dimensional Transition Metal Carbides and Nitrides

Mohammad Khazaei, Masao Arai, Taizo Sasaki, Chan-Yeup Chung, Natarajan S. Venkataramanan, Mehdi Estili, Yoshio Sakka, and Yoshiyuki Kawazoe*

Layered MAX phases are exfoliated into 2D single layers and multilayers, so-called MXenes. Using first-principles calculations, the formation and electronic properties of various MXene systems, M_2C (M = Sc, Ti, V, Cr, Zr, Nb, Ta) and M_2N (M = Ti, Cr, Zr) with surfaces chemically functionalized by F, OH, and O groups, are examined. Upon appropriate surface functionalization, Sc_2C, Ti_2C, Zr_2C, and Hf_2C MXenes are expected to become semiconductors. It is also derived theoretically that functionalized Cr_2C and Cr_2N MXenes are magnetic. Thermoelectric calculations based on the Boltzmann theory imply that semiconducting MXenes attain very large Seebeck coefficients at low temperatures.

1. Introduction

Since the discovery of graphene by Novoselov et al.,[1] the synthesis, properties, and applications of 2D materials has become a leading area of interest in the field of material science and engineering. Using micromechanical exfoliation, single layers of graphene, BN, MoS_2, and WS_2 were prepared from their 3D-layered structures in which the layers are held together via van der Waals interactions.[2] The obtained single layers are invariably accompanied by thicker flakes, which hamper the mass production of monolayers for technological applications.[3] As a feasible procedure for large-scale production of 2D materials, an innovative alternative has been developed recently based on a combination of chemical modification and ultrasonic technique.[2–4] Results show that the latter approach can be extended to synthesize 2D monolayers from layered solids.

Previous reports have described that using hydrofluoric acid (HF) solutions and ultrasonic technique, the transition metal carbides, which belong to MAX phase family, e.g., Ti_3AlC_2, Ti_2AlC, and Ta_3AlC_3, can be exfoliated into 2D layers, so-called MXenes.[5–7] MAX phases are a family of layered solids with metallic properties, of which the chemical compositions are given by the formula $M_{n+1}AX_n$, where n = 1, 2, or 3, "M" represents an early transition metal, "A" denotes A group (mostly groups 13 and 14) elements, and "X" can be carbon or nitrogen.[8–14] As an example, **Figure 1**a presents a typical structure of M_2AX systems. In this family of materials, the chemical bonds between A–M elements are weaker than M–X–M bonds, which makes it possible to remove the "A" element from the 3D solid. Accordingly, the solid is exfoliated into 2D layers (Figure 1b). Depending on the applied hydrophobic acid solution, the surfaces of these layers are chemically terminated/functionalized with a different/selective group such as hydroxyl (OH) or fluorine (F).[5,6]

As described in this paper, performing a set of first-principle calculations for many different potential MXene systems clarifies that because of the low dimensionality of MXenes, their electronic and magnetic properties differ greatly from those of their corresponding MAX phase solids upon an appropriate chemical surface treatment by acceptor groups (F, OH, and O). Calculations show that Ti_2CO_2, Hf_2CO_2, Zr_2CO_2 and Sc_2CF, $Sc_2C(OH)_2$, and Sc_2CO_2 are semiconducting with band gaps between 0.24 to 1.8 eV. Thermoelectric calculations show that the MXene semiconductors described above can attain large Seebeck coefficients at low temperatures of around 100 K. Moreover, results reveal that Cr_2CF_2, $Cr_2C(OH)_2$, Cr_2NF_2, $Cr_2N(OH)_2$, and Cr_2NO_2 can be magnetic at low temperatures.

2. Computational Details

Here, first-principles calculations are performed within the context of density functional theory using the generalized gradient approximation with the Perdue–Burke–Ernzerhof (PBE)[15] exchange–correlation functional and the projected augmented wave (PAW) approach with plane wave cutoff energy of 520 eV, as implemented in the VASP code.[16] The positions of atoms, lattice parameters, and angles are fully optimized using conjugate gradient method. Therefore, the maximum force acting on each atom becomes less than 0.005 eV/Å. The criterion for energy convergence is 10^{-6} eV/cell. During optimization, $12 \times 12 \times 1$ k points are used.[17] The partial occupancies are

Dr. M. Khazaei, Dr. M. Arai
National Institute for Materials Science (NIMS)
1-1 Namiki, Tsukuba 305-0044, Ibaraki, Japan
E-mail: khazaei.mohammad@nims.go.jp
Dr. T. Sasaki, Dr. M. Estili, Prof. Y. Sakka
National Institute for Materials Science (NIMS)
1-2-1 Sengen, Tsukuba 305-0047, Ibaraki, Japan
Dr. C.-Y. Chung, Dr. N. S. Venkataramanan, Prof. Y. Kawazoe
Institute for Materials Research (IMR)
Tohoku University, Sendai 980-8577, Miyagi, Japan

DOI: 10.1002/adfm.201202502

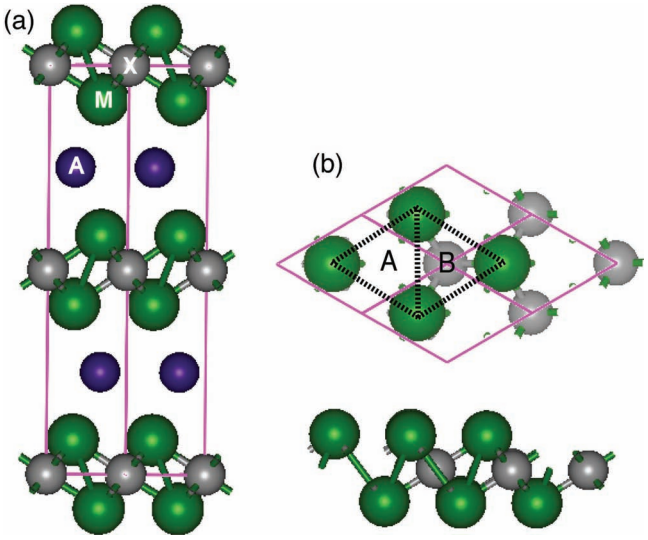

Figure 1. a) Typical bulk structure of layered M_2AX solid, where M, A, and X represent the transition metal, A-element, and carbon/nitrogen atoms, respectively. b) Top and side views of the obtained 2D M_2X layer. The dotted lines exhibit the A-type and B-type hollow sites described in the text. For simplicity, only the first and second layers of the M_2X are shown in the top view.

determined using the Methfessel–Paxton smearing scheme with smearing width of 0.1 eV.[18] To avoid any interaction between an MXene sheet and its periodically repeated images along the *c* axis, a large vacuum space of 30 Å is used. After structural optimization, the density of states (DOS) and electronic properties of the layers are calculated using 42 × 42 × 1 *k* points. The thermoelectric Seebeck coefficients are obtained based on the Boltzmann theory[19] implemented in BoltzTrap code.[20,21] BoltzTrap is useful for assessing the thermoelectric properties of both metallic and semiconducting systems. However, the current version of this code is restricted to analyses of nonmagnetic systems.[20,21]

3. Structural Models

To predict the novel and general electronic properties of MXenes, we have studied the geometrical structures and electronic and magnetic properties of a series of potential MXene systems systematically, although only a few have been synthesized experimentally. The development of some others is still in progress.[5,6] We constructed appropriate models for 2D MXene systems by removing the "A" element (Al, Si, Ga, In, and Sn) from the bulk MAX phases. To simplify the discussion, we specifically examine M_2X MXenes (M = Sc, Ti, Zr, Hf, V, Nb, Ta, Cr; X = C or N), which are the thinnest MXene systems among the others. Finally, we intend to present our general observations about thicker MXene systems. After elimination of the "A" element, it is expected that the created metal surfaces are terminated chemically. In fact, it has been observed experimentally that the outer layers are terminated with F and/or OH groups when the MXenes are chemically exfoliated by HF acid solutions. It might also be possible to produce O-terminated surfaces under chemical conditions, or by post-processing of OH-terminated systems, for example by thermal treatment or ultraviolet-ozone cleaning technique. Therefore, we consider the MXene systems in which the surfaces are terminated by F, OH, and O groups.

An M_2X system consists of trilayer sheets with a hexagonal-like unit cell, where the X (C or N) layer is sandwiched between the two "M" transition metal layers, as shown in Figure 1b. Because the coordination number of a transition metal ion is often six, a similar atomic configuration by a chemical group for an MXene system can be inferred, thereby implying the formation of M_2XF_2, $M_2X(OH)_2$, and M_2XO_2. The reason for the full surface termination is discussed later. On an M_2X surface, hollow sites of two types exist, as shown in Figure 1b: hollow sites A, for which no "X" atom is available under the transition metals; and hollow sites B, for which an "X" atom is available. Therefore, according to the relative positions of the attached termination groups to the metal atoms, four configurations are possible for the chemical terminations of an M_2X system: Model 1 has two functional groups located on the top of the two transition metals; Model 2 has two functional groups on top of the hollow sites A; Model 3 has one functional group located on the top of the hollow site A and the other functional group locates on the top of a hollow site B; and Model 4 has two functional groups located on the top of hollow sites B. These models are shown in **Figure 2**. For each type of functionalization, we have fully optimized the atomic coordinates.

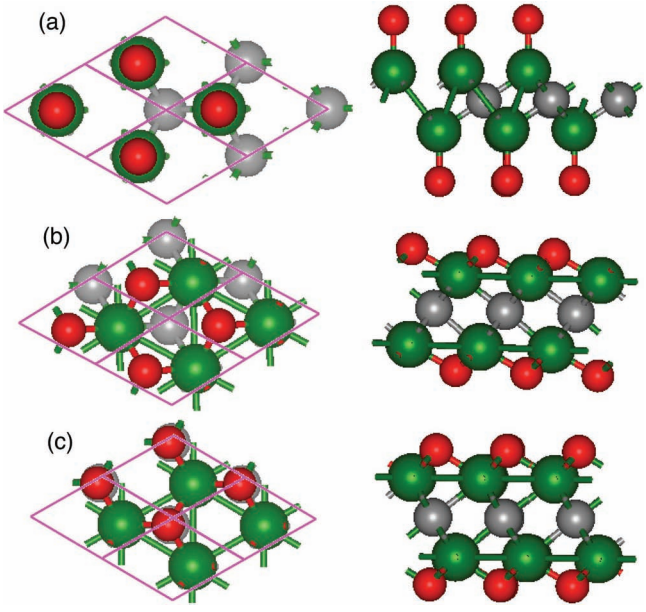

Figure 2. a–c) Top and side views of models of the functionalized MXene systems. a) Model 1, b) model 2, and c) model 4. Model 3 is not shown because its faces resemble models 2 and 4. Green, gray, and red balls show positions of transitional metals, the carbon/nitrogen atoms, and the attached functionalized groups, respectively. Here, the *z*-direction (*c*-lattice direction) is the normal vector to the MXene surfaces. For simplicity, only the first and second layers of the M_2X are shown in the top view.

Table 1. Total energy of models 1–4 for M_2C (M = Sc, Ti. V, Cr, Zr, Nb, Ta) and M_2N (M = Ti, Cr, Zr) systems chemically functionalized by F, O, and OH. The most stable model is highlighted in bold-typeface.

M_2C or M_2N	F	OH	O
Sc_2C			
1	−37.87	−49.12	−40.61
2	**−37.87**	**−49.12**	−40.61
3	−37.29	−48.75	**−41.22**
4	−36.66	−48.35	−41.083
Ti_2C			
1	−39.34	−51.03	−43.68
2	**−39.36**	**−51.03**	**−44.46**
3	−39.15	−50.91	−43.69
4	−38.82	−50.72	−42.71
Ti_2N			
1	−39.91	−51.66	−44.84
2	**−39.92**	**−51.66**	**−45.40**
3	−39.50	−51.40	−44.87
4	−39.50	−51.40	−44.25
Zr_2C			
1	−41.21	−52.82	−46.35
2	**−41.21**	−52.80	**−46.99**
3	−41.13	**−52.82**	−46.12
4	−40.89	−52.69	−45.03
Zr_2N			
1	−41.47	−53.13	−47.72
2	**−41.47**	**−53.20**	**−47.72**
3	−41.12	−53.01	−47.28
4	−41.32	−53.13	−46.62
Hf_2C			
1	−44.04	−55.88	−50.77
2	**−44.07**	**−55.88**	**−50.77**
3	−44.04	**−55.88**	−49.78
4	−43.79	−55.73	−48.58
Hf_2N			
1	−42.51	−55.93	−50.82
2	−43.87	−55.92	**−51.29**
3	−43.63	−55.77	−50.82
4	**−43.95**	**−55.93**	−50.11
V_2C			
1	−38.20	−50.12	−41.76
2	**−39.10**	**−50.97**	**−44.03**
3	−38.59	−50.58	−43.77
4	−38.68	−50.73	−43.40
Nb_2C			
1	−40.10	−52.08	−47.08
2	**−41.39**	**−53.26**	**−47.09**
3	−40.91	−52.92	−46.91
4	−41.17	−53.21	−46.57
Ta_2C			
1	−43.97	−55.95	−51.46
2	**−44.62**	−56.70	**−51.46**
3	−44.15	−56.33	−51.29
4	−44.56	**−56.75**	−50.89
Cr_2C			
1	−37.26	−49.38	−41.00
2	**−37.71**	**−49.59**	−42.53
3	−37.50	−49.45	−42.59
4	−37.14	−49.19	**−42.71**
Cr_2N			
1	−36.96	−49.12	−40.87
2	**−38.13**	**−49.90**	**−43.35**
3	−38.13	−49.82	−43.00
4	−38.11	−48.75	−43.05

Continues

4. Results and Discussion

The results of total energies for all models and functionalizations are presented in **Table 1**. Our optimization results show that, generally speaking, model 1 is energetically less stable than any of the other three considered models. In many cases, it is transformed to a model of 2–4.

To ascertain the stability of the functionalized MXene sheets in the experiments, we have calculated their formation energies, defined as

$$\Delta H_f = E_{tot}(M_2XY_n) - E_{tot}(M_2X) - (n/2)E_{tot}(Y_2) - n\Delta\mu, \quad (1)$$

where M_2X represents the pristine MXenes without functionalization, and Y = F, OH, or O groups. The number of chemical groups in the super cell is *n*, which is 2 for the current form. $E_{tot}(M_2X)$ and $E_{tot}(M_2XY_n)$ respectively stand for the total energies of pristine and functionalized MXenes. Depending on the functionalization type, $E_{tot}(Y_2)$ is the total energy of F_2, O_2+H_2, or O_2. $\Delta\mu = \mu$-$(1/2)E_{tot}(Y_2)$, where μ is the chemical potential of the attached chemical group, which can vary as a function of pressure and temperature.[22] The results of formation energy calculations at $\Delta\mu$ = 0.0 eV are presented in **Table 2**. That table shows that all formation energies are large negative values, which indicates the formation of strong bonds between the transition metals and the attached groups, engendering the development of MXene systems with a particular surface functionalization.

We have assumed that the MXene surfaces are fully functionalized/terminated by the attached groups, but a question remains as to whether the formations of such systems are thermodynamically favorable with respect to the lesser functionalization. To investigate the thermodynamic feasibility of formation of such systems, we examined the formation energies of Ti_2C systems at different oxygen concentrations and chemical potentials, as defined by Equation 1. We selected Ti_2C because

Table 2 Formation energy of different MXene systems functionalized with F, OH, and O groups at $\Delta\mu = 0.0$ eV.

MXene systems	F	OH	O
Sc_2C	–12.14	–10.48	–9.35
Ti_2C	–10.85	–9.61	–9.81
Ti_2N	–10.68	–9.51	–9.49
Zr_2C	–11.26	–9.95	–10.90
Zr_2N	–10.94	–9.75	–11.05
Hf_2C	–11.183	–10.09	–11.74
Hf_2N	–10.55	–9.62	–11.75
V_2C	–9.30	–8.26	–8.09
Nb_2C	–9.36	–8.32	–8.92
Ta_2C	–9.03	–8.26	–9.73
Cr_2C	–8.04	–7.00	–6.89
Cr_2N	–8.61	–7.47	–7.70

its 2D sheets have been produced experimentally and because it is representative of MXene systems with interesting electronic and thermoelectric properties, as shown later. We constructed a 2×2 model of Ti_2C containing eight Ti and four carbon atoms, and functionalized both sides surfaces of it with 1 (lowest concentration) to 8 (highest concentration) oxygen atoms in a super cell. For each oxygen concentration, many different possibilities exist. We have considered more than 100 structures of $Ti_8C_4(O_2)_{n/2}$ systems, n = 1–8. The formation energies of each oxygen concentration are shown in **Figure 3** as a function of the chemical potential between –6.0 to 0.0 eV. That figure shows that in a very wide range of chemical potentials between –4.0 and 0.0 eV, the structure with full oxygen coverage (with 8 oxygen atoms) is thermodynamically the most favorable configuration among all configurations with lower oxygen concentrations. The chemical potential is estimated as varying from 0 to –0.8 eV in the temperature range of 230–750 K.[22] Therefore, the full termination is the most stable configuration under such a condition. Moreover, we have calculated the phonon spectra

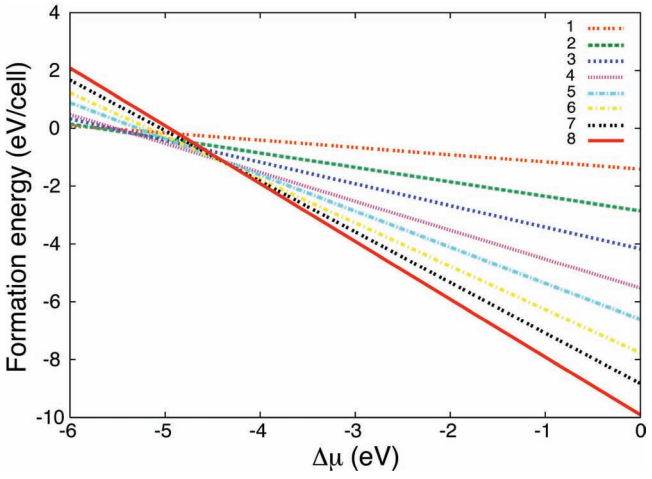

Figure 3. Formation energies of a 2×2 Ti_2C model consisting of 1–8 oxygen atoms as a function of the oxygen chemical potential.

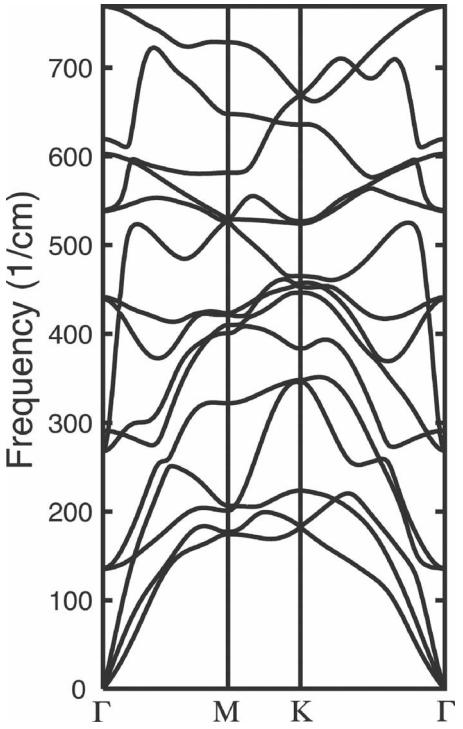

Figure 4. Phonon dispersion frequencies of Ti_2CO_2.

of the fully terminated Ti_2C with oxygen atoms, as shown in **Figure 4**. Results show that all phonon frequencies are positive, signifying that this system is in its equilibrium state. Therefore, it can be expected that various fully functionalized MXenes are realized in the experiment.

Furthermore, we have investigated the electronic properties of the most stable structure of each functionalized MXene system. Although most of the MXenes are metallic, results show that Sc_2CX_2 (X = F, OH, and O), Ti_2CO_2, Zr_2CO_2, Hf_2CO_2 are semiconducting. The energy gaps were obtained, respectively, as 1.03, 0.45, and 1.8 eV for Sc_2X_2 (X = F, OH, and O), and 0.24, 0.88, and 1.0 eV for Ti_2CO_2, Zr_2CO_2, Hf_2CO_2. From the calculated band structures (**Figure 5**), it is inferred that $Sc_2C(OH)_2$ has a direct band gap and that other semiconductors have indirect band gaps. Ti, Zr, and Hf are in the same group in the periodic table with the same number of electrons in their outer shells ($[Ar]3d^24s^2$, $[Kr]4d^25s^2$, and $[Xe]4f^{14}5d^26s^2$). Therefore, the corresponding MXene systems exhibit similar metallic to semiconducting behaviors near the Fermi energy upon the same type of functionalization. In addition, it is predicted that both F and OH groups similarly affect the electronic structure of a pristine MXene system because each of the F and OH groups can receive only one electron from the surface. The O group might differ from F and OH because it demands two electrons from the surface to be stabilized at its adsorption position, as discussed in greater detail below.

To ascertain why these MXenes are semiconductors and why others are metallic, we systematically investigated how the electronic structures of pristine MXenes change upon different functionalizations. Our calculations show that all pristine M_2X systems are metallic, while their Fermi energies locate at the d

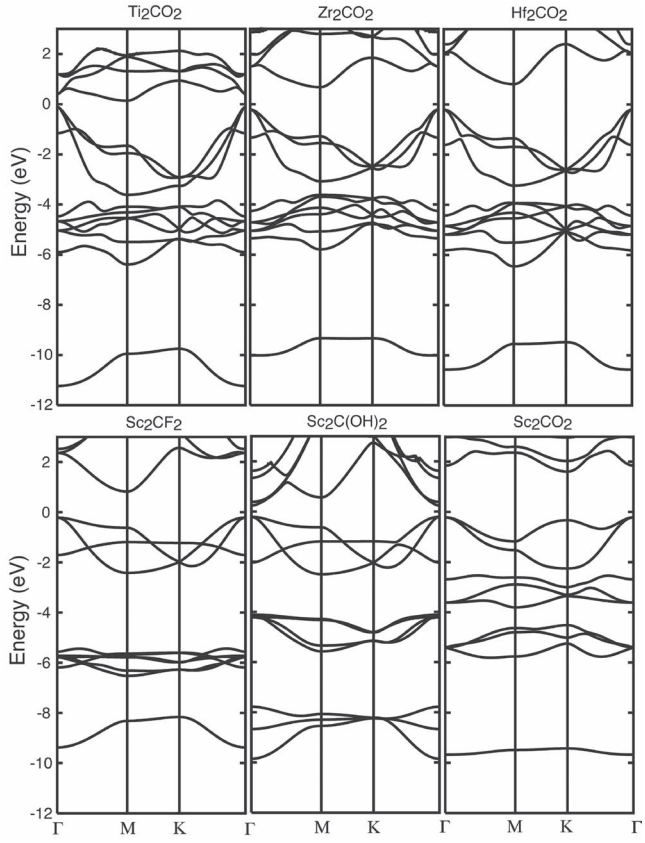

Figure 5. Band structure of semiconducting MXene systems. The Fermi energy is at zero.

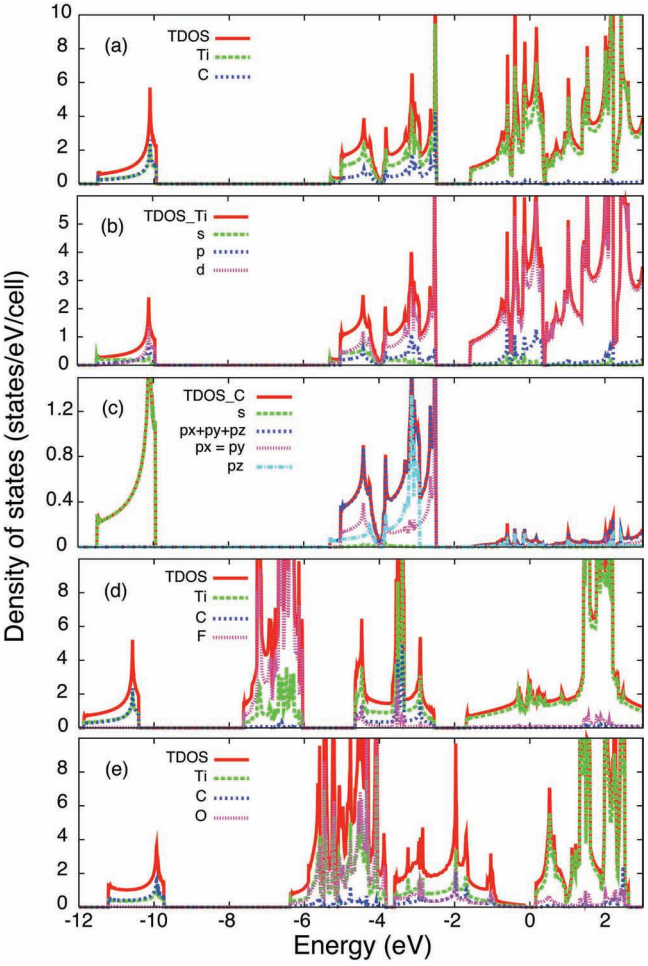

Figure 6. a) DOS of Ti_2C, b,c) the PDOS on atomic orbitals of Ti and C atoms, respectively. d,e) DOSs of Ti_2CF_2, and Ti_2CO_2, respectively. Fermi energy is at zero. For the semiconductors, it is shifted to the center of the gap.

bands of the transition metals. In most MXenes, the p-bands of carbon/nitrogen appear below the d-bands of transition metals separated by a small band gap. In all considered functionalized MXene systems, it is observed that, because of the lower electronegativity of the transition metals than the X (C and N) atom and the attached functional groups, the transition metals become positively charged by donating their electrons to both X atoms and the attached groups. As an interesting example of MXene systems, the effect of different functionalization on Ti_2C is considered below.

Figures 6a–c show the total and projected densities of states (TDOS and PDOS) of pristine Ti_2C. As seen in Figures 6a and b, the pristine Ti_2C is a metallic system, whereas the energy states around the Fermi energy are mainly made of the Ti-d orbitals. From Figures 6b and c, it is apparent that the C p-orbitals form the energy bands hybridized with Ti d-orbitals (between −3.0 and −5 eV), which are separated by a gap of around 1.0 eV from the Ti d-bands. The band at −10.0 eV comprises C s- and Ti s,d-orbitals.

As might be readily apparent from Figure 6d, when the F groups are adsorbed onto the Ti_2C surfaces, each F atom obtains one electron from Ti_2C, and the Fermi energy shifts downward, but the Ti_2C remains metallic after F functionalization. Furthermore, additional bands are produced by F-p and Ti-d around −7.0 eV. When O groups are adsorbed onto the Ti_2C surface, each O atom receives two electrons from Ti_2C such that the Fermi energy shifts downward to the center of the gap separating Ti-d and C-p bands, see Figure 6e, which explains why Ti_2C, Zr_2C, and Hf_2C become semiconducting upon O functionalization. Hybridized O p- and Ti d-orbitals are formed around −5.0 eV. In the semiconducting systems described above, the transition metals (Ti, Zr, and Hf) reach their maximum oxidation number by donating their electrons and becoming positively ionized (+4), but oxygen and carbon atoms become negatively charged (−2 and −4, respectively) by receiving additional electrons as a nominal valence. Because Ti atoms can provide sufficient electrons for both C and the attached F, OH, or O groups, model 2 is an appropriate model for them because the anion and the cations attract each other effectively. As described above, after either F or O functionalization, new states are created below the Fermi energy. They result from the hybridization of Ti d-orbitals with F p-orbitals/O p-orbitals. A similar discussion is applicable to the case of the Sc_2C system. The total energies indicate that the preferred structure for Sc_2CF_2/$Sc_2C(OH)_2$ is model 2, while that for Sc_2CO_2 is model 3. This difference is explained as follows.

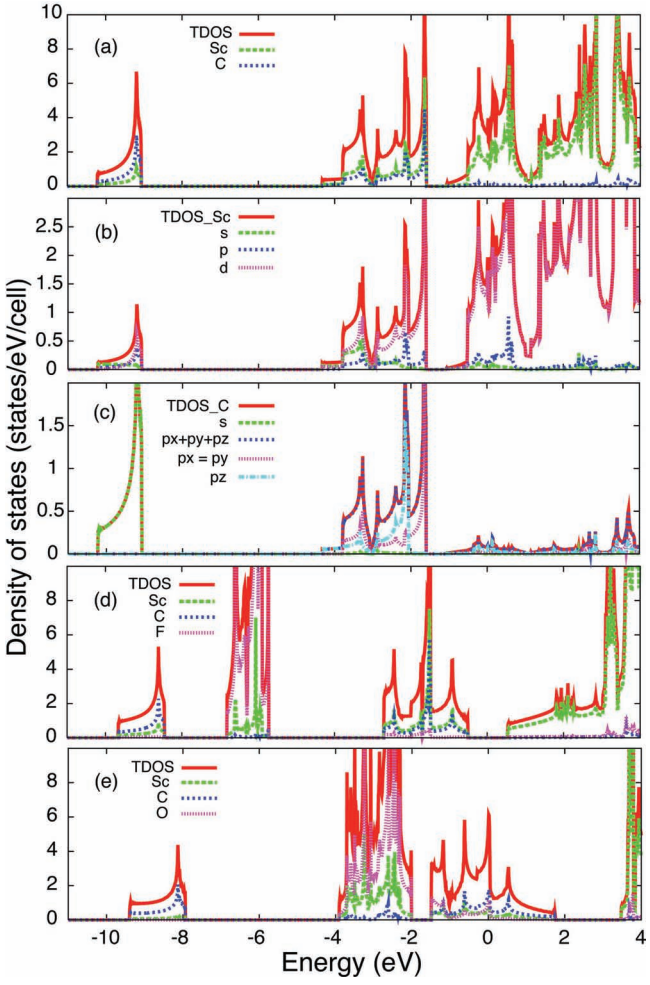

Figure 7. a) DOS of Sc_2C, b,c) PDOS on atomic orbitals of Sc and C atoms, respectively. d) DOS of Sc_2CF_2. e) DOS of model 2 of Sc_2CO_2. Fermi energy is at zero. For the semiconductors, it is shifted to the center of the gap.

As might be apparent from **Figures 7**a,b similar to the Ti_2C case the Fermi energy of pristine Sc_2C locates in the Sc-d bands. Figures 7b,c show that the hybridized C p- and Sc d-bands are separated from the Sc d-bands with a gap of around 0.5 eV. It is noteworthy that the maximum oxidation state of Ti is +4, whereas the maximum oxidation state of Sc is +3. Therefore, in contrast to the Ti_2C case, upon F or OH functionalization, the Fermi energy of Sc_2C shifts to the center of the gap and Sc_2CF_2 and $Sc_2C(OH)_2$ turn out to be semiconducting, see Figure 7d. In these systems, each Sc atom is positively charged (+3), while C (-4), F (–1), and OH (–1) are negatively charged. Sc atoms can provide sufficient electrons for both C and the attached F or OH groups. Therefore, the calculations show that model 2 becomes an appropriate structural model for Sc_2CF_2 and $Sc_2C(OH)_2$.

Sc_2C functionalized with oxygen is an interesting case because O needs more electrons than either F or OH, although the Sc atoms cannot provide sufficient electrons for both attached O groups. At first glance, one might expect that upon O functionalization, the Fermi energy shifts downward, rendering Sc_2CO_2 as a metallic system. This might be true, as shown in Figure 7e, if it is assumed that the most stable structure for Sc_2CO_2 is model 2. However, the total energy calculations show that model 3 is an appropriate structural model for Sc_2CO_2, which indicates that because Sc atoms cannot provide sufficient electrons for an oxygen group, the oxygen prefers to move on the top of the hollow site, where a carbon atom is available under it, i.e., the B-type hollow site. The electronic structure of model 3 is discussed below.

TDOS and PDOS of model 3 of Sc_2CO_2 are shown in **Figure 8**. To clarify the discussion, we separately displayed the PDOS of two Sc atoms (Sc_A and Sc_B) and two O atoms (O_A and O_B) in the unit cell of Sc_2CO_2. O_A (O_B) are the O atoms adsorbed onto A-type (B-type) hollow sites, whereas the Sc_A (Sc_B) are the Sc atoms located near O_A (O_B). The O p-orbitals mainly contribute to the energy bands between –6.5 to –3.0 eV, which we interpret as O p-bands. Because of the different local configurations, they split into two parts with the O_B p–bands from –6.5 to –5 eV and the O_A p-bands from –4.5 to –3 eV. They both hybridize with Sc d-orbitals because three Sc atoms with distance of 2.085 Å (2.101 Å) between Sc_A (Sc_B) and O_A (O_B) surround the O atoms. Furthermore, results show that the O_B p_z-orbital is hybridized with the C p_z-orbital. The distance between O_B and C is 1.65 Å, which is shorter than that of O_B and Sc_B. This hybridization forms the anti-bonding states of C p_z and O_B p_z at 1.0–1.5 eV.

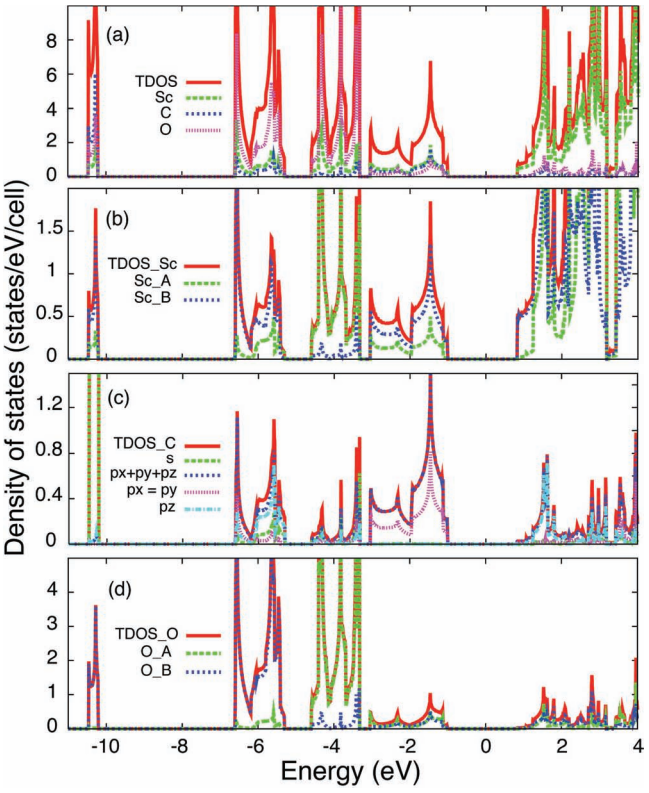

Figure 8. a) DOS of model 3 of Sc_2CO_2. b–d PDOS on atomic orbitals of Sc, C, and O atoms, respectively. Sc_A/Sc_B denotes Sc atoms, which make A-/B-type hollow sites. O_A/O_B represents the O atom adsorbed onto A-/B-type hollow site. Fermi energy is at zero. For semiconductors, it is shifted to the center of the gap.

Therefore, Sc_2CO_2 becomes an insulator because of the splitting of these unoccupied anti-bonding states. In brief, it is observed that the O atoms are adsorbed onto atomic sites, where they can acquire their necessary electrons by hybridization, which explains why model 3 became favorite models for Sc_2CO_2. It is predicted that, because of the asymmetric surfaces of Sc_2CO_2, it might be observed as scrolled structures in the experiments. MXenes with scrolled structures have already been observed in experiments.[5] As a general trend, it can be predicted that the relative structural stabilities of models 2–4 depend mainly on the possible ionic state(s) of the transition metals on the surfaces. Regarding the oxidation states of transition metals, if the transition metals can provide sufficient electrons for both X and the attached functional groups, then model 2 becomes the most stable configuration; otherwise either of model 3 or 4 would be a more stable configuration.

In relation to the electronic structures of thicker MXene sheets with a larger number of transition metals, Ti_3C_2, Ti_4C_3, Ti_5C_4, Ti_4N_3, V_3C_2, V_4C_3, Nb_4C_3, Nb_4C_4, Ta_3C_2, and Ta_4C_3, results show that these systems remain metallic upon any type of the functionalization. Similar to graphene and graphite structures, the MXenes can also be prepared experimentally in single-layer or multilayer forms. Therefore, in addition to single layers, we have also constructed multilayered structures of MXene systems for this study. After full structural optimizations, it is predicted that the multilayers of many MXene systems can be made. In most of the studied multilayers, the distance between the top of a MXene sheet to the bottom of the next sheet is around 3.0 Å, indicating that the sheets are bound mainly by van der Waals interaction. We have also studied the electronic structures of the prepared MXene multilayers. However, no marked difference was apparent between their electronic properties with their corresponding single sheets at near Fermi energy. It is noteworthy that a theoretical study was conducted by Enyashin and Ivanovskii on the electronic structure of $Ti_2C(OH)_2$ and $Ti_3C_2(OH)_2$ systems in which the layers are folded into nanotube forms. They found that all the studied nanotubes have metallic-like character.[23]

As an interesting possible property of the MXene systems, we examined the thermoelectric Seebeck coefficient of MXenes based on the Boltzmann theory. Our calculations showed that the semiconducting MXene systems will exhibit very large Seebeck parameters at low temperatures. As an example of these systems, we showed the Seebeck coefficient of Ti_2CO_2 at different temperatures and electron chemical potentials in **Figure 9**a. At low temperatures of around 100 K, Ti_2CO_2 acquires a large Seebeck coefficient of about 1140 μV/K. Our calculations have shown that MXene systems with a larger semiconducting gap, for example $Sc_2C(OH)_2$, gain larger Seebeck coefficients at the same temperature in comparison to the others, see Figure 9b. The large thermoelectric Seebeck coefficients of semiconductors are usually attributed to the large contrast of DOS and/or carrier velocities above and below the electron chemical potential, particularly near gap edges.[24,25] The argument above is valid for the case of Ti_2CO_2, see Figure 6e, which has a very large/low DOS at the bottom of the conduction band/top of the valence band. The Seebeck coefficients of the semiconducting MXene systems are predicted to be comparable to the reported giant Seebeck coefficient of $SrTiO_3$ (850 μV/K around 90 K).[26] It is noteworthy that although the Seebeck coefficient is an important parameter for discovering a good thermoelectric material with high figure of merit, it is not the only one. In addition to the Seebeck parameter, the electrical conductivity (σ) and thermal conductivity κ (= κ_l+k_e) with both lattice (κ_l) and electronic (k_e) contributions significantly affect the figure of merit of a thermoelectric material.[21]

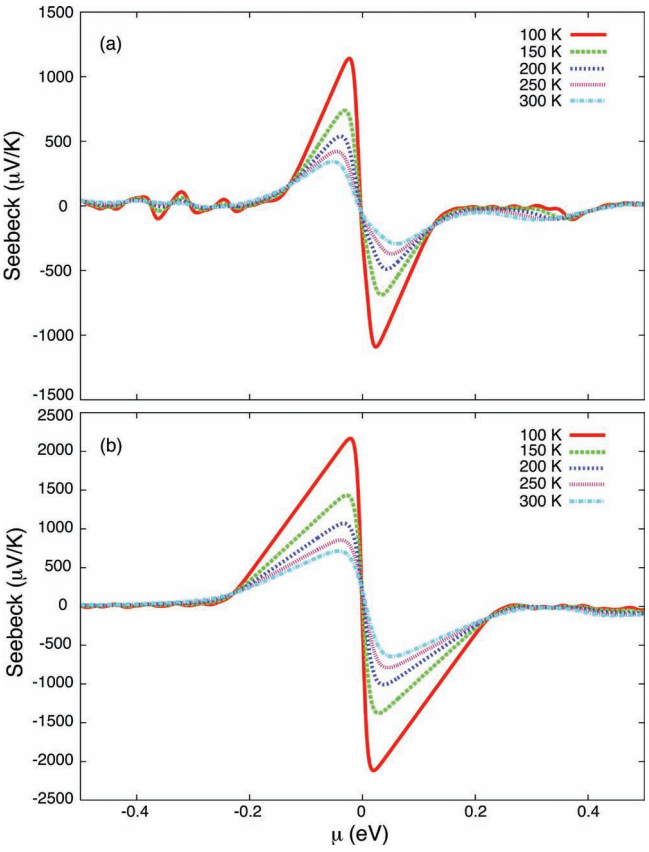

Figure 9. Calculated Seebeck coefficient of a single layer of Ti_2CO_2 (a) and $Sc_2C(OH)_2$ (b) as a function of electron chemical potential at different temperatures. Edges of valence and conduction bands of Ti_2CO_2 are located at –0.12 and 0.12 eV, and for $Sc_2C(OH)_2$ are located at –0.225 and 0.225 eV.

Many Cr compounds are magnetic. Hence, we performed structural optimization of Cr_2C and Cr_2N systems with spin-polarized GGA/PBE method. Our calculations indicate that the ground states of the functionalized Cr_2C and Cr_2N systems are ferromagnetic, as shown in **Table 3**,[27] whereas the ground states of majority of the functionalized MXene systems are nonmagnetic. Our electronic structure calculations have shown that the magnetic properties of these systems result from d orbitals of Cr. The magnetic moments of Cr atoms in these magnetic systems are presented in Table 3. A previous theoretical study of Cr_3SiC_2 shows that Cr atoms might have magnetic moments (0.45 μ_B/Cr) in the bulk MAX phases.[28] Table 3 shows that the energy differences between the magnetic and non-magnetic configurations of the Cr-based MXene are so large that these systems might maintain their magnetic properties nearly up to room temperature. Additionally, it

Table 3. Magnetic properties of Cr_2C and Cr_2N systems, functionalized with F, OH, and O groups. ΔE denotes the energy difference between the total energy of ferromagnetic and nonmagnetic configurations.

	F	OH	O
Cr_2C			
magnetic moment (μ_B/Cr)	2.71	2.24	0.0
ΔE (eV/Cr)	–0.12	–0.08	0.0
Cr_2N			
magnetic moment (μ_B/Cr)	3.23	3.01	2.50
ΔE (eV/Cr)	–0.35	–0.26	–0.49

might be possible to induce/tune the magnetic properties of MXene by strain, as demonstrated for the 2D systems of VS_2 and VSe_2.[29]

5. Conclusions

In conclusion, motivated by recent experimentally obtained results on exfoliation of some of the MAX-phase solids into 2D sheets, so-called MXene, we examined the geometric and electronic properties of the single layers and multilayers of MXenes, when their surfaces are terminated with F, OH, or O groups. Our calculations show that fully functionalized MXenes are mechanically and thermodynamically stable systems. Without surface functionalization, all the MXenes are metallic. Upon functionalization, however, Sc_2CF_2, $Sc_2C(OH)_2$, Sc_2CO_2, Ti_2CO_2, Zr_2CO_2, and Hf_2CO_2 become semiconductors with energy gaps around 0.25–2.0 eV. The ground states of Cr_2CF_2, $Cr_2C(OH)_2$, Cr_2NF_2, $Cr_2N(OH)_2$, and Cr_2NO_2 are ferromagnetic. Narrow-gap semiconductors are usually good thermoelectric materials. Therefore, we have also examined the thermoelectric Seebeck coefficients of our designed MXene sheets. Results show that the monolayers of semiconducting MXenes yield very large Seebeck parameters that are at, or higher, than 1140 μV/K at temperatures around 100 K. Our simulation results provide new insights into possible applications of MXene systems in future nanoelectronic technology and encourage researchers to undertake new studies in this field.

Supporting Information

Supporting Information is available from the Wiley Online Library or from the author.

Acknowledgements

The authors would like to thank Dr. S. Suehara for reading the manuscript and for his constructive comments and helpful discussions.

Received: August 31, 2012
Published online: December 4, 2012

[1] K. S. Novoselov, D. Jiang, F. Schedin, T. J. Booth, V. V. Khotkevich, S. V. Morozov, A. K. Geim, *Proc. Natl. Acad. Sci. USA* **2005**, *102*, 10451.
[2] J. N. Coleman, M. Lotya, A. O'Neill, S. D. Bergin, P. J. King, U. Khan, K. Young, A. Gaucher, S. De, R. J. Smith, I. V. Shvets, S. K. Arora, G. Stanton, H.-Y. Kim, K. Lee, G. T. Kim, G. S. Duesberg, T. Hallam, J. J. Boland, J. J. Wang, J. F. Donegan, J. C. Grunlan, G. Moriarty, A. Shmeliov, R. J. Nicholls, J. M. Perkins, E. M. Grieveson, K. Theuwissen, D. W. McComb, P. D. Nellist, V. Nicolosi, *Science* **2011**, *331*, 568.
[3] R. Mas-Ballesté, C. Gómes-Navarro, J. Gómez-Herrero, F. Zamora, *Nanoscale* **2011**, *3*, 20.
[4] M. A. Bizeto, A. L. Shiguihara, V. R. L. Constantino, *J. Mater. Chem.* **2009**, *19*, 2512.
[5] M. Naguib, M. Kurtoglu, V. Presser, J. Lu, J. Niu, M. Heon, L. Hultman, Y. Gogotsi, M. W. Barsoum, *Adv. Mater.* **2011**, *23*, 4248.
[6] M. Naguib, O. Mashtalir, J. Carle, V. Presser, J. Lu, L. Hultman, Y. Gogotsi, M. W. Barsoum, *ACS Nano* **2012**, *6*, 1322.
[7] M. Naguib, J. Come, B. Dyatkin, V. Presser, P.-L. Taberna, P. Simon, M. W. Barsoum, Y. Gogotsi, *Electrochem. Commun.* **2012**, *16*, 61.
[8] M. W. Barsoum, *Prog. Solid State. Chem.* **2000**, *28*, 201.
[9] D. Music, Z. Sun, R. Ahuja, J. M. Schneider, *Phys. Rev. B* **2006**, *73*, 134117.
[10] Z. Sun, D. Music, R. Ahuja, S. Li, J. M. Schneider, *Phys. Rev. B* **2004**, *70*, 092102.
[11] J. Emmerlich, D. Music, A. Houben, R. Dronskowski, J. M. Schneider, *Phys. Rev. B* **2007**, *76*, 224111.
[12] D. Music, Z. Sun, J. M. Schneider, *Solid State Commun.* **2005**, *133*, 381.
[13] M. Dahlqvist, B. Alling, J. Rosén, *Phys. Rev. B* **2010**, *81*, 220102.
[14] Y. L. Du, Z. M. Sun, H. Hashimoto, M. W. Barsoum, *J. Appl. Phys.* **2011**, *109*, 063707.
[15] J. P. Perdew, K. Burke, M. Ernzerhof, *Phys. Rev. Lett.* **1996**, *77*, 3865.
[16] G. Kresse, J. Furthmüller, *Comput. Mater. Sci.* **1996**, *6*, 15.
[17] H. J. Monkhorst, J. D. Pack, *Phys. Rev. B* **1976**, *13*, 5188.
[18] M. Methfessel, A. T. Paxton, *Phys. Rev. B* **1989**, *40*, 3616.
[19] G. S. Nolas, J. Sharp, H. J. Goldsmid, *Thermoelectrics: Basic Principles and New Materials Developments*, Springer, Berlin, Germany **2001**.
[20] G. K. H. Madsen, D. J. Singh, *Comput. Phys. Commun.* **2006**, *175*, 67.
[21] J. Yang, H. Li, T. Wu, W. Zhang, L. Chen, J. Yang, *Adv. Funct. Mater.* **2008**, *18*, 2880.
[22] W.-X. Li, C. Stampfl, M. Scheffler, *Phys. Rev. B* **2003**, *68*, 165412.
[23] N. Enyashin, A. L. Ivanovskii, *Comput. Theor. Chem.* **2012**, *989*, 27.
[24] M. Onoue, F. Ishii, T. Oguchi, *J. Phys. Soc. Jpn.* **2008**, *77*, 054706.
[25] L. Hao, T. K. Lee, *Phys. Rev. B* **2010**, *81*, 165445.
[26] H. Ohta, S. Kim, Y. Mune, T. Mizoguchi, K. Nomura, S. Ohta, T. Nomura, Y. Nakanishi, Y. Ikuhara, M. Hirano, H. Hosono, K. Koumoto, *Nat. Mater.* **2007**, *6*, 129.
[27] In Hf_2NF_2 and $Hf_2N(OH)_2$, small magnetic moments were also observed around 0.29 and 0.14 μ_B/Hf, but the energy differences between their ferromagnetic and nonmagnetic configurations were very small <-0.006/Hf atom.
[28] W. Luo, C. M. Fang, R. Ahuja, *Int. J. Mod. Phys. B* **2008**, *22*, 4495.
[29] Y. Ma, Y. Dai, M. Guo, C. Niu, Y. Zhu, B. Huang, *ACS Nano* **2012**, *6*, 1695.